



Treball Final de Grau

**Control of lyotropic cholesteric liquid crystals by means of
magnetic fields and chiral dopants**

**Control de cristalls líquids liotròpics cromònics mitjançant camps
magnètics i dopants quirals**

Berta Martínez Prat

June 2016



UNIVERSITAT DE
BARCELONA

B:KC Barcelona
Knowledge
Campus
Campus d'Excel·lència Internacional

Aquesta obra esta subjecta a la llicència de:
Reconeixement–NoComercial–SenseObraDerivada



<http://creativecommons.org/licenses/by-nc-nd/3.0/es/>

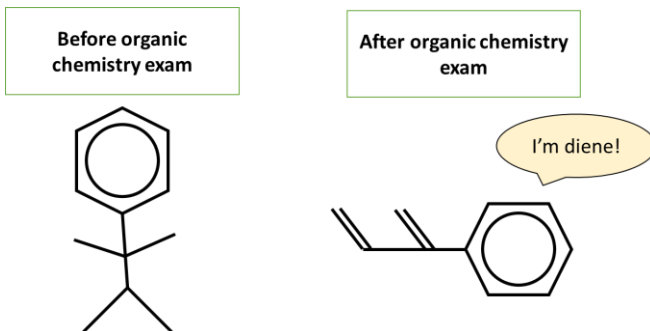
Only a few know, how much one must know to know how little one knows.

Werner Heisenberg

Estrès i cansament, les dues sensacions que un sent quan està acabant una carrera i , com tots sabem, això causa que una estigui susceptible o “arísca”, com diria el meu pare. Així és com he estat aquests últims dies. Tot i així, les persones del meu voltant com la meva família i els meus amics i, en especial, el meu germà (que, no sé per què em fa treure el geni que no trec amb ningú més) han seguit suportant-me i arrancant-me somriures. Per això, els hi ho voldria agrair. A part, també m’agradaria donar les gràcies a en Pau i en Josep que m’han ajudat al llarg de la realització d’aquest treball i han aguantat les meves fantàstiques bromes (hauria de ser monologuista en lloc de química, ho sé).

Finalment, agrair també el suport rebut per part d’en Francesc Sagués i el meu tutor Jordi Ignés que m’han introduït en el fantàstic món dels cristalls líquids i de la biofísica (tot i que aquí no parli de tal disciplina).

Abans de començar posaré un acudit perquè qui comenci a llegir aquest treball ho faci amb un somriure i el vegi ja d’una altra manera:



REPORT

CONTENTS

1. SUMMARY	3
2. RESUM	5
3. INTRODUCTION	7
3.1 Liquid crystals (LCs)	7
3.1.1 Classification of LCs	8
3.1.2 LC phases	8
3.2 Lyotropic liquid crystals	10
3.2.1 Lyotropic amphiphilic LCs	11
3.2.2 Lyotropic chromonic liquid crystals (LCLCs)	11
3.3 Sunset Yellow (SY)	12
3.4 Distortions of the director field in nematic LCs	14
3.5 LC anchoring	15
3.6 Anisotropy	15
3.6.1 Optical anisotropy	15
3.6.2 LCs under external fields	16
3.7 Drops of nematic LCs	17
3.8 Optical characterization of LCs	20
3.8.1 Polarized light	20
3.8.1.1 Phase retardation	21
3.8.2 Polarized optical microscopy (POM)	21
4. OBJECTIVES	23
5. RESULTS AND DISCUSSION	25
5.1 Configuration of SY drops	25
5.1.1 Characterization of twist angle	27
5.2 Configuration of SY drops under a magnetic field	28
5.3 Configuration of SY drops with a chiral dopant	31

5.3.1 Pitch quantification of SY chiral nematic	32
6. EXPERIMENTAL SECTION	35
6.1 Preparation of SY solutions	35
6.1.1 SY purification	35
6.1.2 SY solutions	35
6.1.3 SY and Brucine sulfate solutions	35
6.2 Preparation of LC cells	35
6.2.1 Glass cleaning, PVA coating and glass rubbing	35
6.2.2 LCs cell assembly	36
6.2.3 Cell's thickness measurements	37
6.2.4 Control of temperature	38
6.2.5 Application of a magnetic field	38
6.3 SY nematic drops characterization	38
6.3.1 Twist angle measurements	39
6.3.2 Pitch measurements	39
7. CONCLUSIONS	43
8. REFERENCES AND NOTES	45
9. ACRONYMS	47
APPENDICES	49
Appendix 1: Defects in nematic drops	51
Appendix 2: Twist angle characterization method	53

1. SUMMARY

Over the last decades, a kind of aqueous based liquid crystals (LCs) has extended the field of conventional LCs. This kind of LCs is the so-called lyotropic chromonic liquid crystals (LCLCs). LCLCs present different appealing properties, such as biological compatibility, which have led to a growing interest among the scientific community.

One of the most typical LCLCs is the azo dye Sunset Yellow (SY). Here, we report a study of SY nematic droplets coexisting with its isotropic phase. Furthermore, we describe a control of these droplets via chiral dopants and magnetic fields.

With this study we aim to provide a better understanding of SY drops and, thus, give the opportunity to make new functional materials such as polymer-dispersed liquid crystals (PDLCs). These materials have been discovered relatively recently and that hold promise for several optical applications such as switchable windows or image projectors.

Keywords: Liquid crystals, lyotropic chromonic liquid crystals, nematic drops, twisted bipolar drops, chiral dopant, magnetic field.

2. RESUM

Durant les darreres dècades, un tipus de cristall líquid (LC) basat en aigua ha permès expandir el camp dels LC convencionals. Aquest tipus de cristalls líquids s'anomenen cristalls líquids liotròpics cromònics (LCLCs). Els LCLCs presenten un gran nombre d'atractives propietats, com per exemple que són biocompatibles. Això ha permès un creixement del seu interès dins de la comunitat científica.

Un dels LCLCs més típics és el colorant Sunset Yellow (SY). Amb aquest projecte donem a conèixer l'estudi que s'ha realitzat sobre les gotes nemàtiques del Sunset Yellow en coexistència amb la seva fase isotròpica. A més, en aquest treball també s'ha descrit una manera de controlar aquestes gotes mitjançant camps magnètic i un dopant quiral.

Amb aquest estudi pretenem donar un millor coneixement de les gotes del SY i, d'aquesta manera, donar l'oportunitat de crear nous materials funcionals tals com els cristalls líquids dispersos en polímers. Aquests materials es van descobrir fa relativament poc temps i són potencialment prometedors per a la fabricació d'elements òptics com els vidres intel·ligents o els projectors d'imatges.

Paraules clau: Cristalls líquids, cristalls líquids liotròpics cromònics, gotes twisted bipolars, dopant quiral, camp magnètic.

3. INTRODUCTION

3.1 LIQUID CRYSTALS (LCs)

Scientists specialized in LCs have always had the same problem: when explaining what they work with, everyone stares at them in puzzlement. A LC? This seems to be an oxymoron. But yes, LC deserve this name, as they are substances that, despite presenting a liquid state (they can flow), have certain order, either positional or orientational in their nanoscale structure.

The first time LCs were observed was in 1888, when the Austrian chemist Friedrich Reinitzer was working with a cholesterol based substance in order to determine its structure. When he was measuring its melting point, he saw that this compound presented two melting points: it passed from a transparent clear liquid to a cloudy liquid before solidification. Despite purifying the substance, no changes were observed. It has to be remembered that at that time, pure substances were thought to have just one melting and one fusion point.

With the help of the physicist Otto Lehman, they observed that this cloudy liquid presented a kind of order in its structure. After some studies, a new concept was finally introduced: liquid crystal or crystalline fluids.^{1, 2}

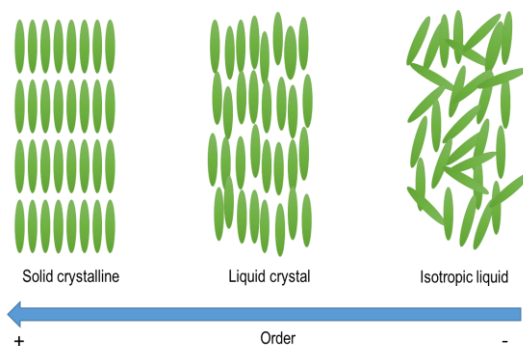


Figure 1. Schematic comparison between the order of a solid crystalline, a LC and an isotropic liquid.

3.1.1 Classification of LCs

LCs can be classified in two main groups: the first one is comprised of thermotropic LCs while the other one includes lyotropic LCs. They differentiate one from the other in the fact that the first ones can be organized by themselves while the others need to be with a solvent in order to be organized. Furthermore, thermotropic LCs depend mainly on the temperature, while lyotropic LCs not only depend on the temperature, but also on the concentration.¹

We will talk more about lyotropic LCs in section 3.2 since the experimental studies have been carried out with one of these LCs.

3.1.2 LC phases

There are some different phases that LCs can display. It is interesting to comment that these phases are extensively known as mesophases or mesomorphic phases and both nouns are formed by the prefix *meso* that means between, in the middle, halfway (i.e. mesophase indicates between phases). Another word composed of this prefix is mesogens which is assigned to the molecules forming mesophases.

A possible classification of mesomorphic phases is listed here:¹

- **Nematic phases**

Nematic is the simplest mesophase as it only presents an orientational order because there is a preferred direction at which the mesogens are on average orientated. This direction determines the director \mathbf{n} , which is equivalent to $-\mathbf{n}$, and the ensemble of all the \mathbf{n} directors form the \mathbf{n} director field. The director \mathbf{n} and the director \mathbf{n} field have to be kept in mind as they will appear repeatedly throughout this project.

The nematic phase is the one studied in our experimental work. More specifically, we have studied some properties of nematic drops of a given LC. This is why a more detailed description of nematic drops is provided in section 3.7.

- **Cholesteric phases**

In the case of cholesteric phases (also known as chiral nematics), the LC performs just an orientational order, like nematics, but with the difference that the \mathbf{n} director changes along the so-called twist or helicoidal axis. These kinds of mesophases can be seen in chiral molecules that self-assemble or in achiral molecules mixed with a chiral compound, called chiral dopant.

The resulting cholesteric phase can be characterized by the pitch, which is the distance over which the LC undergoes a 360° twist.

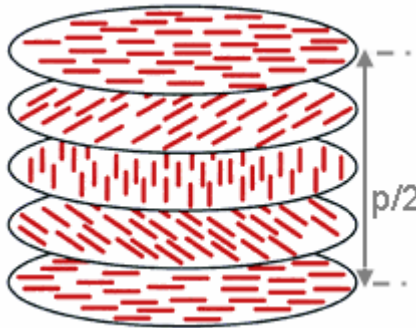


Figure 2. Schematic representation of the half of a pitch of a cholesteric phase
(Benutzer Heimoponnath, 31/6/2016 via Wikimedia Commons, Creative Commons Attribution)

- **Smectic phases**

These mesophases are characterized by their high order on the molecular scale. Apart from possessing orientational order, the molecules are also organized in layers, i.e. smectic phases also have positional order. This arrangement in layers makes the smectic phases have a high viscosity.

- **Columnar phases**

In this type of mesophases, the molecules are stacked in columns of one dimension which can be arranged in many different ways. An example is the columnar hexagonal phase, in which the columns are disposed in such a way that they display a hexagonal lattice.

- **Hexagonal phases**

This kind of mesophase is seen in lyotropic amphiphilic LCs (see section 3.2) that form cylindrical micelles which in turn are disposed creating a hexagonal lattice.

- **Lamellar phases**

As hexagonal mesomorphic phases, lamellar phases are exclusive of lyotropic amphiphilic LCs and are created with stacked bilayers (or lamellae).

- Micellar phases

In this case, the mesophase is composed of spherical micelles displaying different lattices such as body-centered cubic lattices.

Not all the kinds of LCs perform all these mesophases. In Table 1 the most common mesophases for lyotropic and thermotropic LCs are summarized:

<u>Phases commonly observed depending on the type of LC</u>	
Type of LC	Phase
Thermotropic	Smectic phases
Thermotropic and lyotropic	Nematic phases
	Cholesteric phases
	Columnar phases
Lyotropic	Hexagonal phases
	Micellar phases
	Lamellar phases

Table 1. Most common mesophases for each type of LC.

3.2 LYOTROPIC LIQUID CRYSTALS

As it was previously mentioned, lyotropic liquid crystals are formed by at least two components: a solute and a solvent (generally water); contrary to thermotropic LCs which, in general, are pure substances.

The most extensively studied and the first discovered lyotropic LCs are the lyotropic amphiphilic LCs. However, other types of lyotropic LCs also exist. An example is lyotropic chromonic liquid crystals (LCLCs) which have been creating a growing interest among the scientific community, due to their appealing characteristics. For example, recent studies have remarked their potential in biological sensing applications as they are biologically friendly.^{3, 4} Other applications in which LCLCs have a potential interest are optical polarizers, optically anisotropic films, nano-fabrication materials and organic electronics.

First of all, we will describe lyotropic amphiphilic LCs and then we will go into detail with LCLCs as our experimental section is about one of these LCLCs.

3.2.1 Lyotropic amphiphilic LCs ¹

As their name indicates, lyotropic amphiphilic LCs are formed by amphiphilic substances. These compounds present two parts with very different affinity, being one part hydrophobic whereas the other is hydrophilic. So that, the molecules self-assemble in order to keep the hydrophobic part far from the water.

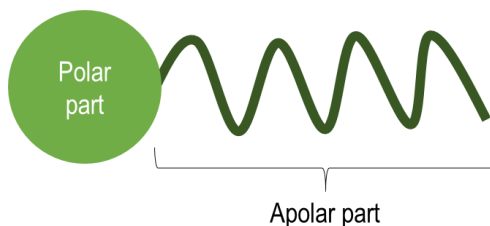


Figure 3. Schematic representation of the structure of an amphiphilic molecule

At very low concentrations, the amphiphilic molecules are dissolved in the bulk of the solvent. Then, they start to be adsorbed in a thin film at the air-solvent interface and an equilibrium is established between the molecules dissolved and the ones adsorbed. When the concentration is increased further, the surface gets saturated and the molecules start to gather, forming aggregates –also called micelles- in the bulk of the solvent. These aggregates can have different shapes - not necessary spherical- that depend essentially on the molecular structure of the amphiphile.

At higher concentrations, the interactions between the micelles become more important and the aggregates start forming mesomorphic states. Hence, unlike thermotropic LC, whose fundamental unit is a molecule in itself, the fundamental unit in lyotropic LC is a micelle, formed by the union of hundreds of molecules.

3.2.2 Lyotropic chromonic liquid crystals (LCLCs)

It has been already commented that over recent years, there has been a growing interest in lyotropic chromonic liquid crystals LCLCs. This broad, but not yet well-understood family of lyotropic LCs is formed by drugs, dyes and DNA nucleotides, such as guanosine. The name chromonics is given to this family of LCs to carry connotations of dyes and chromosomes.⁴

LCLCs, despite being lyotropic LCs, differ in almost every aspect from their amphiphilic analogues.

The molecules of aliphatic compounds - which form together with the solvent the lyotropic LC- are, in general, rod-like, unlike the molecules of LCLCs that in general present a disk-like or plank-like structure with an aromatic rigid core and some solubilizing groups around, such as hydrophilic ionic or hydrogen-bonding groups.

Another difference between lyotropic aliphatics and lyotropic chromonics is that for the first ones, the most important driving force to self-assemble are the hydrophobic interactions, while for the second ones it is the π - π stacking, although other interactions such as Van der Waals, hydrophobic and polar are also present.^{4,5} Moreover, LCLC do not form micelles and they do not present a cmc (critical micellar concentration). In fact, LCLCs start to self-assemble at very low concentrations and the aggregates' sizes increase as the concentration increases. Also, it is well known that self-assembly in aliphatic lyotropic LC is entropic driven, while LCLCs' self-assembly appears to be enthalpy driven. The stability of the system solvent-cholesteric is stable, thanks to the electrical repulsions between the ionic or the polar groups.

3.3 SUNSET YELLOW (SY)

Sunset Yellow is a synthetic commercial dye used in food, drugs and cosmetics. In the solid state, this dye is red, contrary to what the reader might have imagined due to its name. Like many dyes, SY is an azo compound, chemical group responsible for its color. Its IUPAC name is Disodium 6-hydroxy-5-[(4-sulfophenyl)azo]-2-naphthalenesulfonate.⁴

This azo compound presents two tautomeric structures: the hydrazone and the hydroxyazo tautomers. After some computational simulations and spectroscopic analysis, it has been established that the most stable tautomer of SY, and hence the most prevailing one in both the dilute solution and the chromonic mesophase, is the hydrazone tautomer.^{5,17}

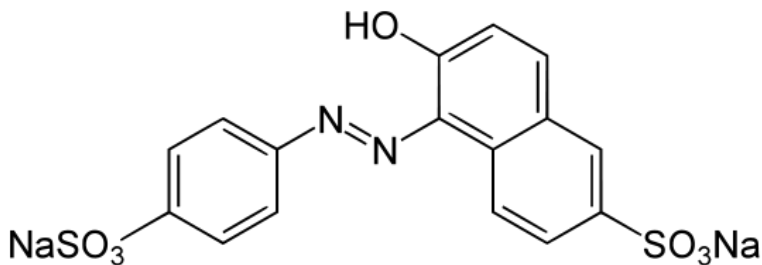


Figure 4. Molecular structure of SY

When SY is dissolved in water, its molecules start to self-assemble into aggregates and, at high concentrations these aggregates are ordered displaying a mesophase. In addition, according to its structure and the way SY self-assembles, this dye can be classified as a LCLC.

It has been said in sections above that LCLC self-assemble principally thanks to the π - π interactions. And so it happens with SY; more specifically, SY aggregates are formed by face-to-face stacking.

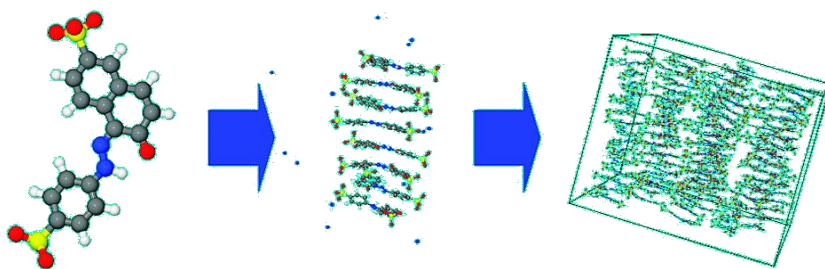


Figure 5. Simulation which represents how the SY molecules self-assemble. The molecules start to form elongated aggregates at very low concentration. Finally, these aggregates self-assemble and form a mesophase beginning from a nematic phase until reaching a columnar phase. (Image extracted from Chami et. al. (ref. 5))

Until now, the mesophases observed in SY solution have been nematic and hexagonal columnar phases. However, the only mesophase studied in our experimental work has been the nematic one.

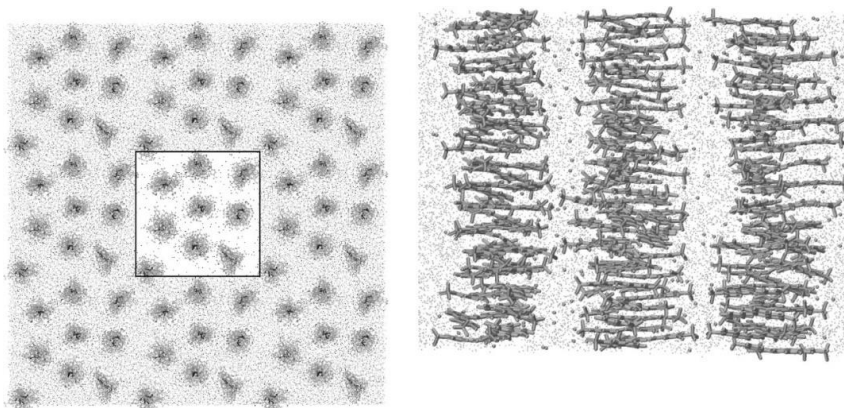


Figure 6. Plan and side view snapshots of the nematic phase taken from a 60 ns molecular dynamics run. (Image extracted from Chami et. al. (ref. 5))

3.4 DISTORTIONS OF THE DIRECTOR FIELD IN NEMATIC LCs

As has repeatedly been said, LCs molecules or aggregates, in the case of lyotropic LCs, present a certain order when displaying a mesophase. The average molecular direction in a nematic mesophase can be represented by a director, \mathbf{n} . If there are no external constraints, this director \mathbf{n} is parallel to a fixed direction throughout the mesophase, since this disposition is the one with minimum energy. However, when there are some external constraints or forces, such as boundary conditions imposed by the container of the mesophase or external fields, the bulk's director field can be distorted.

The distortions can be described by three basic types of deformation: splay, twist and bend. The degree of distortion depends on the elasticity of the material, which is known as nematic elasticity when talking about nematics. This elasticity can be defined with three different constants each one corresponding to one of the three aforementioned deformations. With these three constants, it is possible to determine the so-called Frank-Oseen free energy, which is the energy needed to produce distortions. The smaller these constants are, the lower the energy of deformation.^{1,6}

As a consequence of deformations in the \mathbf{n} director field, there are some points or zones where the mesogens have no way of being disposed, these points or zones are called defects. Defects can be regarded as tears in the order parameter field and if these tears cannot be patched they are known as topological defects. These defects can be seen easily with polarized optical microscopy, since they show as black points or zones in the bulk of a LC.

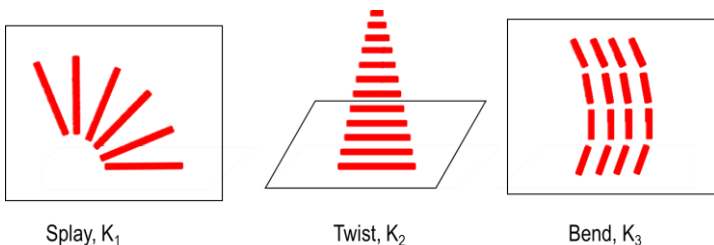


Figure 7. Scheme of the three basic deformations of LCs with their respective constants. Twist is in the 3 dimensions, whereas splay and bend are in 2 dimensions.

3.5 LC ANCHORING ⁷

Interfaces in LCs play a very important role as the **n** director near the surface tends to be oriented in a specific direction. Beyond the surface through the bulk, the structure is gradually recovered with an orientation, although, it has to be remarked that the molecules' alignment on a surface can be propagated over macroscopic distances. Without a surface, nematic orientation can be arbitrary, nevertheless, in the presence of an interface, the orientation is somehow fixed and this orchestrates the global distribution. This fixation of the orientation is known as anchoring.

There are three possible dispositions of the **n** director on a surface:

- **Planar** → the molecules are placed parallel to the surface. There are two possible planar dispositions: homogenous planar (or planar degenerate) when the **n** directors are uniformly orientated over the surface or heterogeneous planar (or planar non-degenerate) in the case of the **n** directors not uniformly orientated over the surface.
- **Homeotropic** → mesogens are perpendicular to the surface.
- **Tilted** → the molecules are positioned at an angle in respect to the surface between 0° (planar) and 90° (homeotropic).

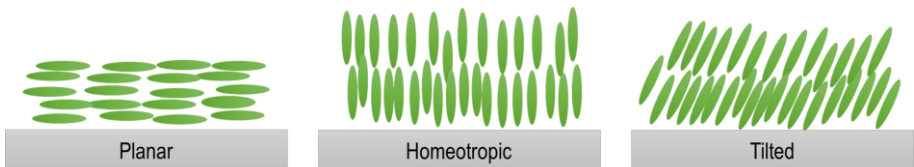


Figure 8. Schematic representation of the different possible anchorings of a liquid crystal at an interface

3.6 ANISOTROPY

Until now, it has been remarked that LCs exhibit an orientational (and sometimes also positional) order. This feature makes LCs anisotropic. Anisotropy is defined as the quality of presenting different macroscopic physical properties (such as the refractive index, the dielectric permittivity, the magnetic susceptibility, the viscosity...) in different directions.^{6, 8}

3.6.1 Optical anisotropy

A phenomenon that emerges from anisotropy is observed when unpolarized light goes through a calcite and it can be seen that an image is doubled. This phenomenon is called

double diffraction and springs up from optical anisotropy (or birefringence). More formally, optical birefringence can be defined as the property of some transparent materials having a refractive index, that depends on the polarization direction or, equivalently, the electric field direction. This property is seen in anisotropic materials; hence it is also observed in mesophases.



Figure 9. A calcite crystal displays the double refractive properties positioned on a sheet of graph paper. (APN MJM, 2/6/2012 via Wikimedia Commons, Creative Commons Attribution)

Anisotropic materials can be either uniaxial or biaxial, although almost all LCs are uniaxial i.e. they are symmetric around one axis. For uniaxial media, birefringence can be quantified as the difference between two normal refractive indexes: the extraordinary (n_e) and the ordinary (n_o) refractive index. The extraordinary refractive index is measured according to the waves with their electric field vibrating along the optical axis. The ordinary refractive index is measured according to the waves with their electric field vibrating perpendicular to the optical axis.

3.6.2 LCs under external fields

It was mentioned previously that when an external field is applied to a LC, some deviations of the \mathbf{n} director field are induced. This is another consequence of LCs' anisotropy as anisotropy induces an alignment of the mesogens.

When an electric field is applied to a LC, the molecules are disposed in such a way that their dipolar moments, which can be either permanent or induced, are parallel to this field. These dipolar moments can lay either parallel (or almost parallel) or perpendicular (or almost perpendicular) to the principal axis of the mesogens. In the first case, molecules would be parallel to the electric field, contrary to the second case, in which the mesogens would be

perpendicular to the field (see Figure 8). This response to the electric field can be quantified by the dielectric anisotropy ($\Delta\epsilon$) which is the difference between the electric permittivity parallel (ϵ_{\parallel}) and the one perpendicular (ϵ_{\perp}) to the long molecular axis.

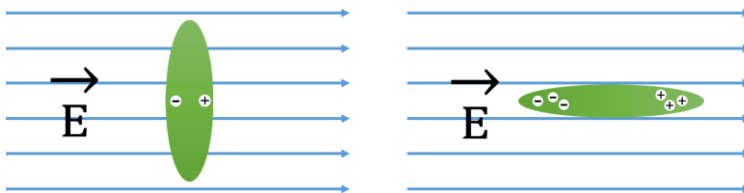


Figure 10. Effect of the applied electric field to anisotropic molecules with negative (a) and positive (b) $\Delta\epsilon$.

This phenomenon can also be seen in the presence of a magnetic field.

Generally, LC organic molecules are diamagnetic, but when applying a magnetic field, a magnetic dipole is induced. This magnetic dipole, in the same way as with the electric dipole, can be produced along or perpendicular to the principal axis of the molecules, so that the molecules are also orientated. The magnetic anisotropy can be quantified as: $\Delta\chi = \chi_{\parallel} - \chi_{\perp}$.

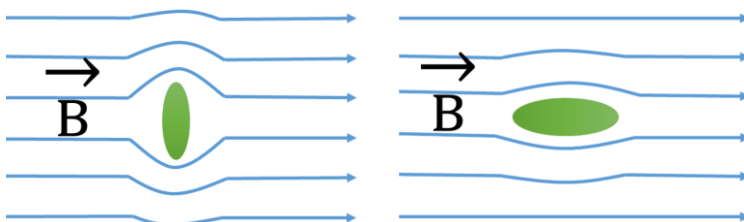


Figure 11. Effect of the applied magnetic field to anisotropic molecules with negative (a) and positive (b) $\Delta\chi$.

The deformation of the \mathbf{n} director field with an electric or magnetic field is known as the Frederick transition. It is called transition because the molecule alignment occurs gradually as the intensity of the applied field increases. The reorientation occurs just when the electric or magnetic field is greater than a threshold value. The external field competes with the elastic forces in the LC and the anchoring at the surface. In general, the molecules at the surface are not aligned with the external field because the interactions at the interface are too strong.

3.7 DROPS OF NEMATIC LCs

Nematic drops can be seen in the coexistence temperature region of the isotropic/nematic phases. At the beginning of the nucleation of the nematic phase in the isotropic phase, the

nematic nucleuses have a spherical shape as an interface is created and this shape allows the minimization of the surface tension. As a consequence, the LC directors have to be adapted to this form. There are many possible configurations that the nematic can adopt, but the equilibrium one springs from the anchoring at the surface and the intrinsic nematic elasticity of the LC. Apart from this, the configuration can also vary in the presence of external forces applied to the LC.

The first thing that one has to take into account in order to figure out a LC drop's configuration is its anchoring, which is supposed to be strong and fixed. As mentioned above, there are two possible anchorings: homeotropic (or perpendicular) and planar (or tangential). The second thing to take into account is the deformation favored, which depends on its elastic constant. Provided that the anchoring, as it has been said, is strong and fixed, the director field of the LC cannot be continuous, hence there must be some deformations ¹. The equilibrium configuration is the one that minimizes the energy. In this way, the distortion that costs less energy, will be the one favored. This does not mean that the other two not-favored deformations will not exist, but they will exist to a lesser degree.

According to these two characteristics, but just considering bend and splay deformations, a general classification of configurations of nematic drops is summarized in the Figure 9:

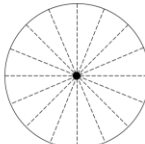
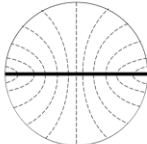
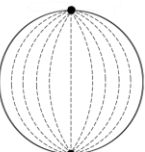
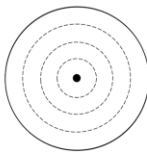
		Favored deformation	
		Splay	Bend
Anchoring	Homeotropic	Radial 	Axial 
	Planar	Bipolar 	Concentric 

Figure 12. The different possible configurations of nematic drops depending on the anchoring and the favored deformation. The figures show the director lines for each configuration.

Obviously, the twist deformation can be also favored so other configurations can arise from the ones already listed e.g. twisted bipolar, twisted radial...

In the case of cholesteric LC there is another configuration called Frank-Price structure. This configuration is seen in cholesterics presenting a tangential anchoring and a high twisting power which is defined as qR where $q=1/P$ (P is the pitch) and R is the drop's radius. When $qR>1$ it's possible to see the Frank-Price structure and with smaller values there are configurations between the twisted bipolar and the Frank-Price one.

The best way to determine the configuration is by observing the defects in the drop.⁹⁻¹¹

- 1- Radial drops present a volume defect called hedgehog and is at the center. A Maltese cross is seen.^{9, 12, 13}
- 2- Bipolar drops have two point surface defects at the ends of the principal axis. These defects are called boojums.^{9, 13, 14}
- 3- Axial drops present a defect ring at the surface.^{9, 15}
- 4- Concentric drops have a disclination at the axis of the drop.^{9, 14}
- 5- Frank-Price drops present a hedgehog defect at the center and a disclination known as Dirac string.^{9, 16}

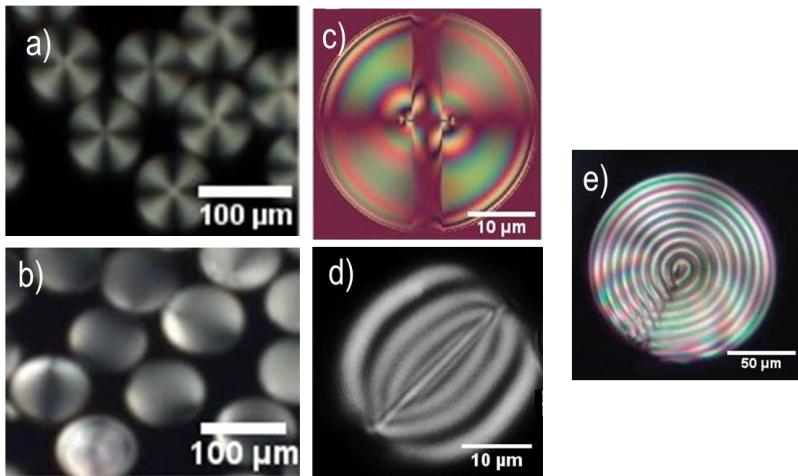


Figure 13. POM images of radial (a), bipolar (b), axial (c), concentric (d) and Frank-Price drops. Images a and b are adapted from Yang et. al. (ref. 12) with permission of The Royal Society of Chemistry, image c is adapted from Aguirre et. al. (ref. 15), image d is adapted from Jeong et. al. (ref. 14) and image e is adapted from Orlova et. al. (ref. 16)

See Appendix 1 to read more about the drops and their defects.

3.8 OPTICAL CHARACTERIZATION OF LCS

3.8.1 Polarized light

When light exits a light source such as a lamp or the sun, this light is unpolarized. This means that the waves that compose this beam of light are vibrating in random directions perpendicular to the light propagation. Nevertheless, when this beam goes through a linear polarizer, it exists as plane-polarized light, this means that there is just one direction of wave vibration. There are also other forms of polarization such as elliptical polarization or circular polarization (which is, in fact, a special case of elliptical polarization). In these cases the polarizers let pass just two normal directions of wave propagation. ^{18, 19}

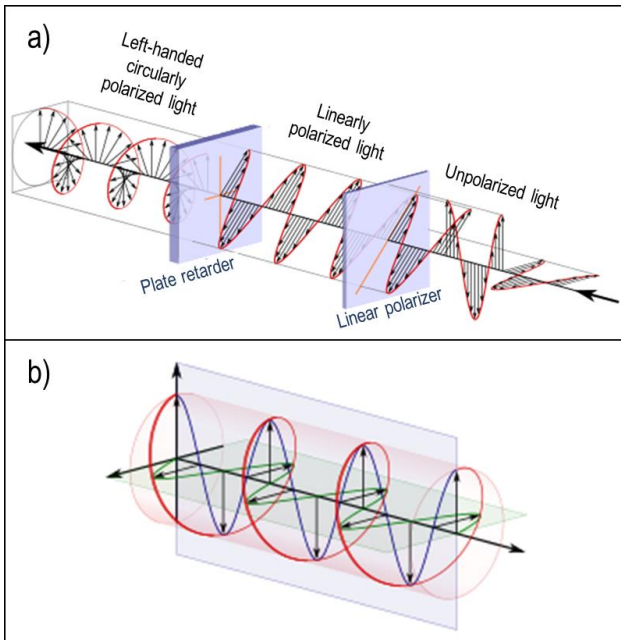


Figure 14. Representation of unpolarized, linearly polarized and left-handed circularly polarized light (a). In b it is possible to see that circularly polarized light can be decomposed into two planar waves. (Dave3457, 6/05/2016 via Wikimedia Commons, Creative Commons Attribution)

3.8.1.1 Phase retardation ^{20, 21}

It has been shown that uniaxial birefringent media possesses two principal refractive indexes (i.e. ordinary refractive indexes, n_o and extraordinary refractive index, n_e) and when unpolarized light goes through an anisotropic media, the beam is split. However, what happens with linearly plane-polarized waves? When linearly polarized light goes through an anisotropic media, it does not travel at the same velocity along the director \mathbf{n} as along the perpendicular director to \mathbf{n} . Hence, initially, when plane-polarized light enters the birefringent media, both polarization components (the one at the fast axis and the one at the slow axis) oscillate in phase, but as they propagate they start to fall out of phase as their velocities are different. This is translated into a phase retardation (or phase shift) when escaping the birefringent material. Optical devices that cause a phase retardation are known as retardation plates or plates retarders.

There are two special cases of phase retardation: when $\Gamma = \pi$ (or multiples), the polarization results in linear polarization and if $\Gamma = \pi/2$ (or multiples) the resulting polarization is circular polarization. In the other cases, the light exiting the retardation plate is elliptically polarized.

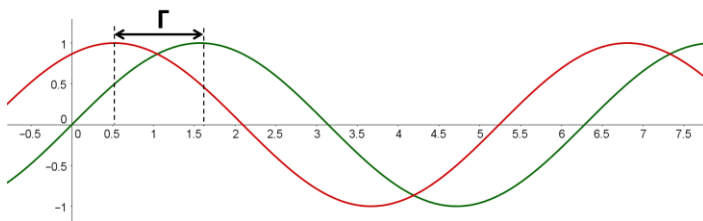


Figure 15. Two different sinusoidal waves with a Γ phase retardation. They have the same amplitude and frequency.

3.8.2 Polarized optical microscopy (POM) ¹⁸

As it has been repeatedly said, LCs are birefringent. This feature makes these substances easily observed with polarized light microscopies. As their name indicates, these devices are based on light polarization and give a great resolution compared with other techniques when observing anisotropic materials. Their most important components are two polarizers placed between the birefringent sample.

When a plane-polarized light beam crosses an anisotropic material this beam experiences a phase shift –as we already said- , then these two split rays when they are recombined produce interferences. These interferences are the fundament of the operating principle of POM as they allow the production the images.

This technique is very useful to differentiate between isotropic and anisotropic media as isotropic media does not split the planar-polarized light. Furthermore, when a birefringent material between two crossed polarizers is rotated, it is seen how the light intensity that arrives to the observer varies. Nevertheless, this phenomenon does not happen with isotropic materials.

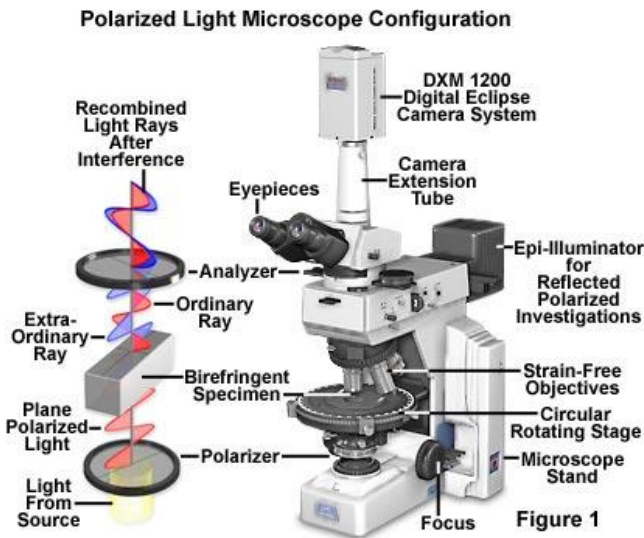


Figure 16. Representation of a polarized optical microscope. Extracted from Robinson et. al. (ref. 18)



Figure 17. The light intensity crossing a system composed of two crossed polarizers with a sample of birefringent material in between varies when rotating the sample. (Image adapted from Murphy et. al. (ref. 20))

4. OBJECTIVES

The main goal of this project has been the creation of a direct and easy strategy for controlling the configuration inside the nematic SY drops. In order to do that, we have used external magnetic fields and a chiral dopant.

The fulfillment of this goal depended in turn on the achievement of other goals:

- Understand the principal properties of LCs.
- Gain a better understanding on nematic drops
- Characterize SY drops without any external control.
- Characterize SY drops under a magnetic field and their response to a rotatory magnetic field.
- Induce a chiral nematic phase to SY drops and its further characterization.

As regards future investigations we also wanted to promote the creation of new materials using SY drops and broaden new horizons in LC applications.

5. RESULTS AND DISCUSSION

5.1 CONFIGURATION OF SY DROPS

In the region of coexistence between the nematic and the isotropic phases, interfaces are created and this costs energy. The way to minimize the surface tension –and hence the surface energy- is by nematic mesophase adopting a spherical shape. Furthermore, the energy needed to create an interface is higher than that needed to break the \mathbf{n} director field uniformity, this is why this spherical shape makes this field distorted. However, SY molecules are disposed in such a way that the total energy of the system is minimized and, as we said before, this equilibrium configuration depends on the three elastic constants and the anchoring on the surface.

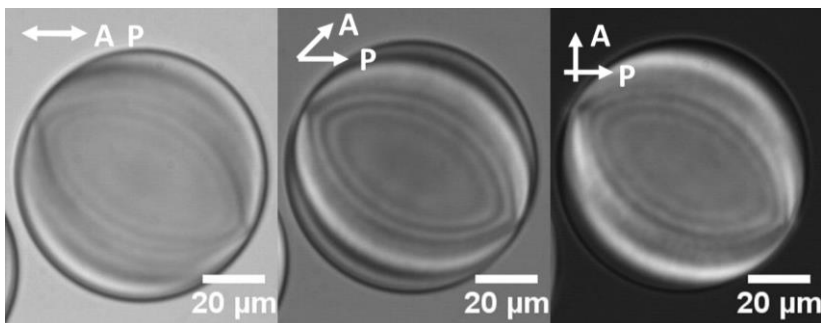


Figure 18. POM images of a nematic SY drop seen at different analyzer (A) – polarizer (P) angles.

First of all, we determined the structure of this droplets. We saw that SY drops had two point defects at the North and South poles of their principal axis (i.e. two Bojoom defects). According to this, the only possible configurations were the bipolar and the twisted bipolar. To differentiate between them, we had to look at the light extinction at the center of a drop depending on the angle between the analyzer and the polarizer. If a drop orientated parallel to the polarizer was purely bipolar, we should have observed a maximum extinction at the center when the polarizers were crossed (i.e. we should see black). This was not the case of SY drops (see

Figure 19). In this way, we could conclude that SY drops displayed a twisted bipolar configuration.

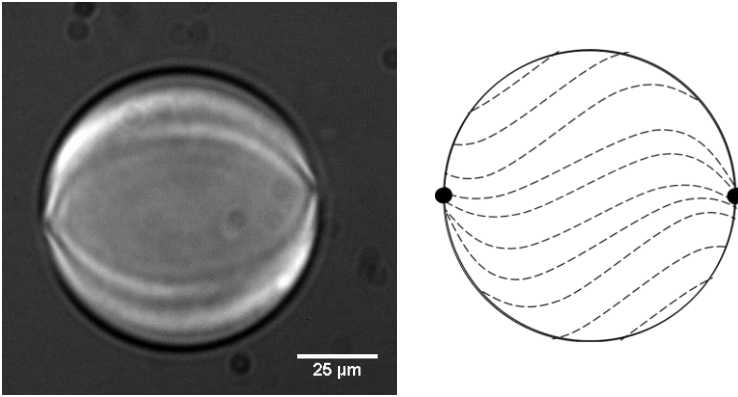


Figure 19. POM image of a nematic SY drop seen between crossed polarizers (left) and a representation of the director \mathbf{n} field in the drop (right)

One possible explanation for why nematic SY drops performed the twisted bipolar configuration is the following one:

It has been said that the equilibrium configuration depends on the surface anchoring and the three elastic constants. The homeotropic anchoring is very difficult to achieve in LCLC unless it is induced via surfactants or other added compounds.²² Here we did not add such substances; so that, concentric and bipolar configurations and their respective twisted configurations were the only ones possible to achieve. If we look at the SY's elastic constants (see Table 2), it is possible to see that the twist constant is much smaller than the splay and bend constants, meaning that twist distortion is much cheaper energetically speaking. In addition, splay distortion is also favored before the bend one. According to these statements, SY drops had to display a bipolar twisted configuration and this is what we observed.

Distortion	Splay	Twist	Bend
Elastic constants (pN)	$K_1 = 4.3$	$K_2 = 0.7$	$K_3 = 6.1$

Table 2. Elastic constants of SY 0.9m T=294 K.

Values extracted from ZHOU et.al. Soft Matter **10**, 6571-6581 (2014)

5.1.1 Characterization of twist angle

Once the configuration was defined, we determined the twist angle, which is the angle that the \mathbf{n} director field twists from the surface onto the principal axis of the drop.

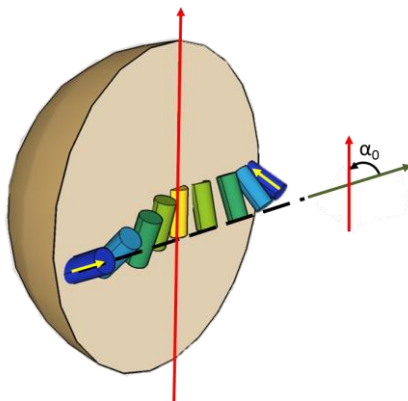


Figure 20. Schematic drawing of the SY aggregates across the drop. The twist angle (α_0) is the angle between the director \mathbf{n} (in yellow) on the surface and the drop principal axis (in red). The drops are supposed to be symmetric around the principal axis; hence, the director \mathbf{n} from this axis towards both opposite surfaces twists the same angle but with different signals.

This parameter was calculated for three different concentrations:

Concentration (m)	Twist angle (degrees)
0.8	97 ± 8
0.9	108 ± 10
1.0	101 ± 8

Table 3. Calculated twist angles for different concentrations of SY.

In general, lyotropic LC's properties change broadly with the concentration; so that, we had expected to find a dependence on the twist angle with the concentration. However, neither tendencies nor significant differences were observed.

One interesting thing to point out is the twist angle signal. This signal gives the direction at which the \mathbf{n} director field twists, indicating the positive values the counterclockwise direction and the negative values the clockwise direction. We measured a total of 14 different drops and 8 presented a positive angle, whereas the other 6 performed a negative one. From this, it is

possible to determine that there is not one preferred twist direction or, said in another way, there is not a preferred handedness of chirality. This is in accordance with what Jeonga et. al. had observed.¹⁴

5.2 CONFIGURATION OF SY DROPS UNDER A MAGNETIC FIELD

It was seen that when applying a magnetic field to the nematic droplets, their configuration changed; they did not present a twisted bipolar anymore. Conversely, they presented a concentric configuration. In this way, the planar anchoring was preserved with the magnetic field, whereas the global structure was changed. This was due to the fact that the anchoring is more energetically expensive than the \mathbf{n} director field deformation.

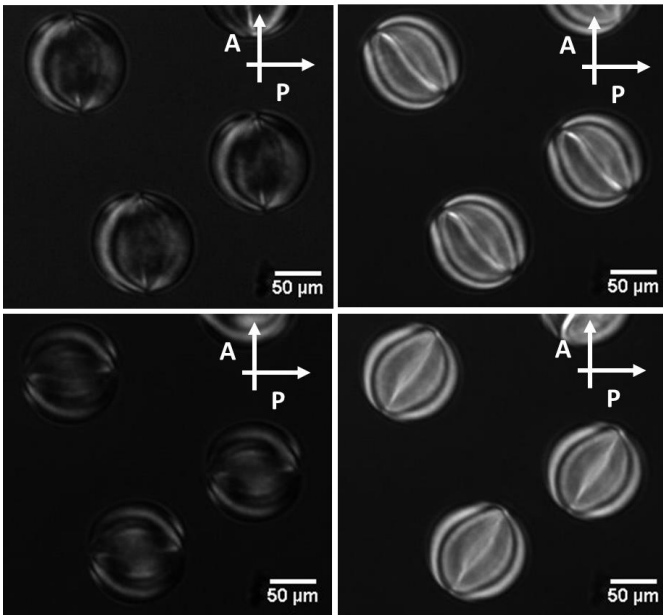


Figure 21. POM images of SY nematic drops under a homogeneous magnetic field oriented at different. This magnetic field lays parallel to the samples' slides. The drops follow the magnetic field aligning their principal axis parallel to the field. These drops display a concentric configuration; hence it is possible to see the disclination at the equator.

It has to be remembered that for SY the bend distortion was the one with a higher elastic constant, hence, it was the one that costed more energy and in the concentric configuration bend distortions were the prevalent one. So now the question is: why do SY drops display this configuration under a magnetic field? The answer is: because of the negative magnetic

anisotropy. This means that the magnetic susceptibility along an aggregate's axis is smaller than the one perpendicular to this axis. In this way, the SY aggregates prefer to be perpendicularly aligned to the magnetic field. By aligning the mesogens in this manner, it is possible to overcome the energetic cost of the bend distortions.

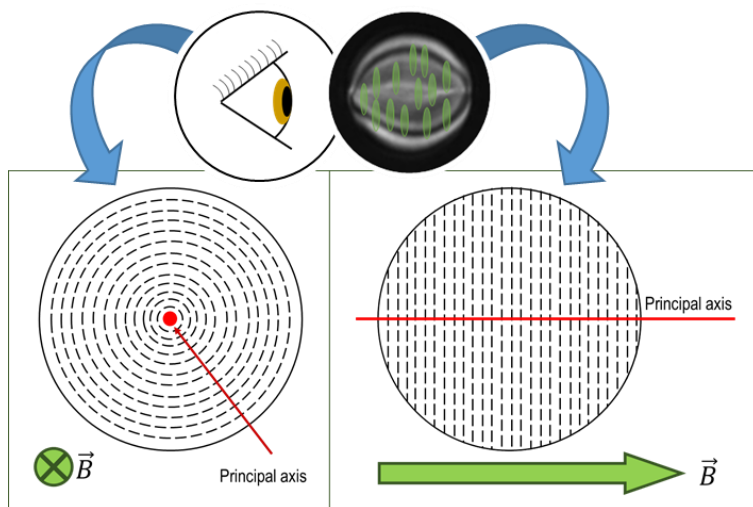


Figure 22. Schematic representation of the concentric drops of SY under a magnetic field seen parallel to the principal axis (right) and perpendicular to the principal axis (left). Notice that SY aggregates are disposed so that they lay perpendicular to the magnetic field.

The major contributors to this magnetic anisotropy are the aromatic rings of SY molecules. It is well known that when a changing magnetic field is applied to a circuit, a current is induced in such a way that it creates a magnetic field that opposes the change, and so happens with diamagnetic compounds: when a magnetic field is applied, it creates an electronic circulation that induces a magnetization which opposes to the applied field. For aromatic compounds such as benzene, the electron delocalization at the molecular plane allows the easy induction of a ring current that creates a magnetic field perpendicular to this plane and opposed to an applied magnetic field. This is the so-called ring current effect. Nevertheless, the induced magnetization at the plane parallel to the molecular plane is weaker, as there is not such electronic delocalization. As a consequence, benzen-like compounds present a magnetic anisotropy, being the susceptibility perpendicular to the molecular plane greater than the parallel one (i.e. they have a positive magnetic anisotropy).

Hence, in order to minimize the magnetic energy, the aromatic rings prefer to stay parallel to the magnetic field. In this way, since SY molecules self-assemble by face-to-face attractions giving aggregates with benzene rings perpendicular to the principal axis, the diamagnetic anisotropy results to be negative ($| \chi_{//} | > | \chi_{\perp} |$ and as $\chi_{//}$ and χ_{\perp} are negative, then $\Delta \chi = \chi_{//} - \chi_{\perp} < 0$). The azo group also induces a diamagnetic anisotropy, but in a much smaller scale.

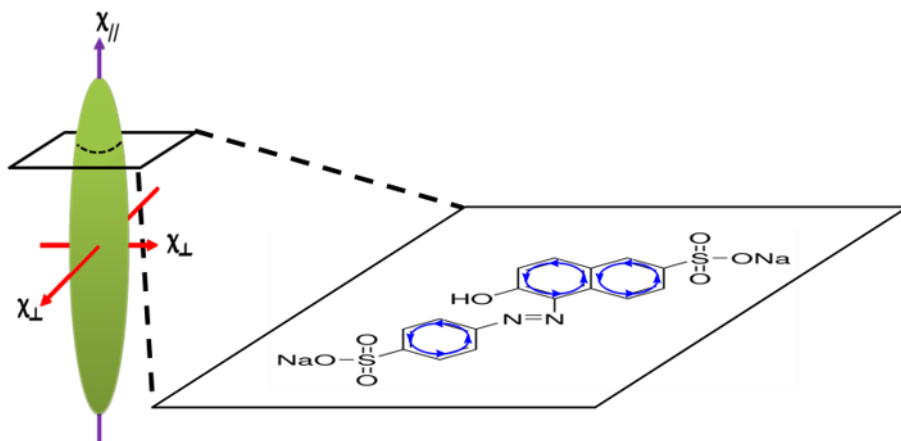


Figure 23. Schematic drawing of a SY aggregate with a negative magnetic anisotropy. The SY molecules lay perpendicular to the principal axis of the drop and, since they have positive magnetic anisotropy, they lead the overall aggregate to have a negative magnetic anisotropy. The positive magnetic anisotropy of SY molecules arises from the ring current effect of the aromatic benzenes. The blue circles represent the ring current.

This response to the magnetic field could be very interesting in optical displays as by rotating the field, it would be possible to tune the light extinction and hence, the light crossing a display made with a SY dispersion.

5.3 CONFIGURATION OF SY DROPS WITH A CHIRAL DOPANT

SY displays nematic and columnar mesophases depending on the concentration and temperature; nevertheless, in the presence of a chiral substance, it presents such characteristics seen in cholesteric LCs. This is because the chiral dopant induces a helicity to the \mathbf{n} director field. One could think that the twist arises from the same principle of the specific optical rotation, but this is completely false. Certainly the twisting in the \mathbf{n} director field emanates from the interaction between the molecules of the chiral dopant and the molecules of the LC.²³ Hence, the cholesteric phase arises from the interplay of anisotropy and chirality.

We studied the influence of a chiral dopant in the SY's nematic mesophase. There are many different chiral compounds which have the ability to induce a chiral nematic LC, but not all of them are equally effective. We chose brucine sulfate as this chiral dopant has been extensively exploited for chirality induction in LC.^{24, 25} However, to the best of our knowledge, up to now, sulfate brucine has not been used with SY mesophases.

It was possible to notice that the cholesteric character increased with the chiral dopant concentration. At high concentrations, the oily streak texture and the Frank-Price drop configuration were observed, both being structures typical from cholesteric mesophases. In this way, we could conclude unmistakably that brucine sulfate induced a chirality in the nematic phase of SY.

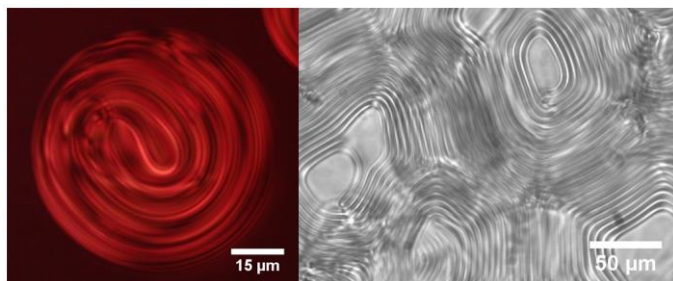


Figure 24. POM images of a Frank-Price configuration drop in the coexistence region between the isotropic and the nematic phase (left) and the oily streak textures in the nematic region of SY/brucine sulfate system.

However, at low concentration these textures could not be seen. This is because the nature of the cholesteric phase depends highly on the dopant's concentration.

Focusing on the drops, we could see that their configuration changed from twisted bipolar at 0 concentration of sulfate brucine to Frank-Price at high concentrations of chiral dopant. At intermediate concentrations, the drops configuration was a half-way between the twisted bipolar and the Franck-Price ones.

In the next figure is it possible to see how changes the drop configuration with the concentration of the chiral dopant.

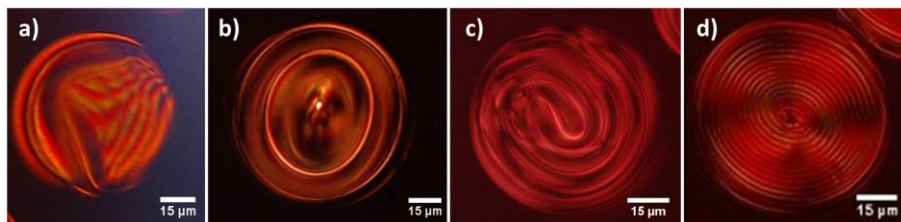


Figure 25. POM images of SY with 0.25% (wt.) (a), 0.6% (wt.) (b), 0.9% (wt.) (c) and 3.1% (wt.) (d) of brucine sulfate. Notice how the chiral nematic character increases with the concentration of the chiral dopant.

One thing interesting to point out is that sulfate brucine induces a preferred handedness chirality, contrary to what was seen in the SY drops without brucine sulfate. We saw that sulfate brucine induced the \mathbf{n} director field to twist in counterclockwise direction. This direction does not have to coincide with the rotation of the plane-polarized light when crossing a brucine sulfate aqueous solution, since, as was already mentioned, the chirality induction is a molecular effect rather than an optic effect like in light rotation.²²

5.3.1 Pitch quantification of SY chiral nematic

In order to characterize and determine the potential of brucine sulfate as a chiral dopant of SY, we measured the pitch at different concentrations of brucine sulfate.

We found that the inverse of the pitch ($q=1/P$) increased linearly with the brucine sulfate concentration (see figure 23). This was in accordance with some other reports.²³⁻²⁵ In fact, it is known that the pitch depends on the concentration as shown in the following equation:

$$P = \frac{1}{c \cdot ee \cdot \beta} \quad \text{Equation 1}$$

where c is the concentration, the ee the enantiomeric excess and β the helical twisting power. This last parameter represents a magnitude of the efficiency of a chiral dopant to induce a chiral mesophase. It has to be remarked that the helical twisting power does not only depend on the chiral dopant, but also on the mesogen, since the helicity is created via interactions between the two different compounds.

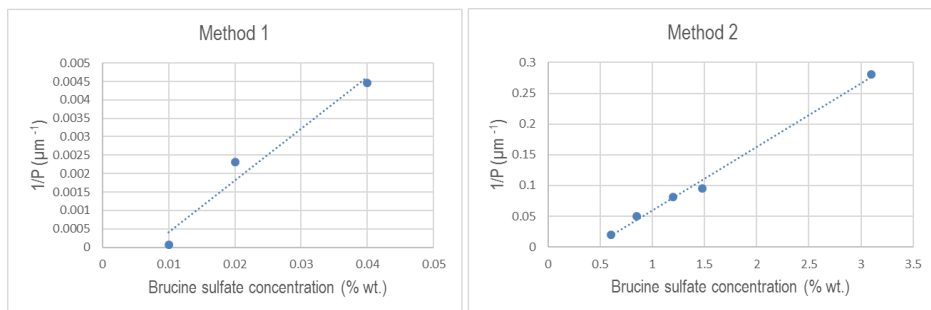


Figure 26. Representation of the inverse of the pitch ($1/P$) in front of the brucine sulfate concentration for both used methods. The slope of the plots corresponds to $ee \cdot \beta$.

	Method 1	Method 2
$ee \cdot \beta$ (μm)	7.10	9.85

Table 4. The $ee \cdot \beta$ values obtained for both methods.

If we look at Table 4, the first thing that one could think is that both values are very different. This difference can be given by the fact that in Method 1 the pitches were determined with samples displaying a nematic mesophase throughout the cell, whereas in Method 2 the pitches were determined directly with the droplets. Hence, anchoring conditions of the chiral nematic were very different from one method to the other and as it was aforementioned, anchoring plays an important role in LCs n director field. Since our aim in this project is to control nematic drops of SY, method 2 fits better to our necessities, however, at very low concentrations this method does not work and if in a future we want to work with LCs with a poor induced chirality, we have to work with very diluted concentrations of sulfate brucine. This is the reason for which we have used both methods.

In addition, theoretically, the pitch should have tended to infinite (i.e. $1/p$ to 0) when the chiral dopant concentration was 0.⁹ However, we found that $1/p$ tended already to 0 with some traces of brucine sulfate. We attributed this to the fact that maybe a threshold concentration is needed in order to induce the chiral mesophase.

Finally, we also calculated the product between $1/P$ (q) and R (the drop's radius), since, as it was explained, Frank-Price configurations arised when qR was greater than 1, so that we calculated this parameter for different drops.

Brucine sulfate concentration (% (wt.))	0.60	0.85	1.20	1.48	3.10
qR	1.0	1.4	2.4	3.3	10.7

Table 5. qR values for different drops at different concentrations of sulfate brucine. The Frank-Price configuration appears from concentrations of 0.6% (wt.) of brucine sulfate.

6. EXPERIMENTAL SECTION

In the subsequent section, a detailed explanation of the proceedings carried out will be provided.

6.1 PREPARATION OF SY SOLUTIONS

6.1.1 SY purification

First to the preparation of the solutions, SY (90% pure from Sigma-Aldrich) was purified by recrystallization in ethanol (96% (v/v) for analysis from Panreac).

6.1.2 SY solutions

Different solutions of Mili-Q water and purified SY at different concentrations were prepared in microtubes wrapped with Parafilm. The solute was dissolved in four cycles of 15 minutes in an ultrasound bath intercalate with 15 seconds in the vortex.

6.1.3 SY and Brucine sulfate solutions

For the solutions with Brucine sulfate, the chiral dopant was first dissolved in water and then SY was added. The Brucine sulfate solutions were prepared from a first 0.9% (wt.) brucine sulfate solution and then, this one was diluted until the desired concentration. All these solutions were prepared in the same way as with the only SY solutions.

6.2 PREPARATION OF LC CELLS

In order to observe properly the LC with the POM, it is important to have a thin film of the LC. The way to achieve it is by sandwiching the LC between two glass slides that, in our case, had to induce a planar anchoring.

6.2.1 Glass cleaning, PVA coating and glass rubbing

Glasses slides were washed first with soap and deionized water. Afterwards they were abundantly rinsed with deionized water. Then, in order to eliminate all possible traces of organic matter, these slides were let in piranha solution (H_2SO_4 (lab grade) + H_2O_2 (30% wt.) from Sigma Aldrich in a relation 3:1) for 1h.

Finally, they were rinsed with Mili-Q water and kept in Mili-Q water until further utilization.

Afterwards, these glass slides were treated depending on the desired LC anchoring.

- PVA coating

As has been remarked, the anchoring between the LC and the substrate is very important as it can orchestrate the global behavior of the mesophase. So that, is important to control this anchoring. The best way to do it is via coating the substrates with polymers.²⁶ Here, we wanted a homogenous anchoring, so that, the polymer chosen was poly(vinylalcohol) (PVA) which is a synthetic polymer with a chemical structure shown in Figure 28.

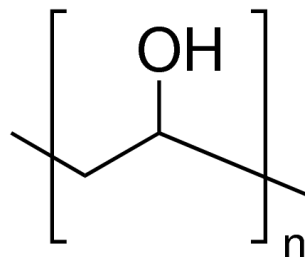


Figure 27. Chemical structure of PVA

A 1% (wt.) PVA solution (88% hydrolysed, average M. W.: 88.000 g/mol, from Acros Organics) solution was spin-coated on glass slides cleaned with piranha solution at a speed of 2800 rpm for 30 s. Once the glass slides were coated, they were heated at 130°C for 2h in order to get rid of water. Finally, they were let to cool down at room temperature.

- Glass rubbing

The best way to have a non-degenerate anchoring is by rubbing the substrate (in our case the glass slides). Rubbing is a mechanical process which consists on scratching the glass with an abrasive surface.²⁶

Glass rubbing was performed with Struers Waterproof Silicon Carbide paper FEPA #220. The glass rubbed had been first cleaned with piranha solution.

6.2.2 LCs cell assembly

The SY solutions were sandwiched between two glass slides, in some cases rubbed glass slides and in another cases PVA-coated glass slides. In order to control the gap between the two substrates, it was used fishing line of 100 μm (Maver Smart SLR Hi-Technology Monofilament Hook Line 0.10 mm of diameter) as spacer. The sample was introduced by capillarity. It was important to avoid the solution's dryness, so that, the cells were sealed with a UV glue (Norland optical adhesive 81 from Norland Products, INC).

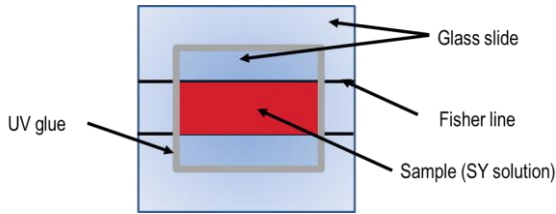


Figure 28. Representation of a LC cell used to characterize SY

6.2.3 Cell's thickness measurements

The cell's thickness had to be known in order to calculate the pitch, the method used was based in the interference that light experiments when is reflected by the glass slides. These interferences were measured by reflections using the SE-Flame-REFLECTANCE VIS reflection spectrometer from Oceanoptics. The interference pattern that the cell shows is the one in Figure 30. The thickness can be calculated with the next equation:

$$d = \frac{M \cdot \lambda_1 \cdot \lambda_2}{2n |\lambda_1 - \lambda_2|} \quad \text{Equation 2}$$

Where, d is the thickness, M the number of maximums or minimums, n the diffraction coefficient and λ_1 and λ_2 the wavelengths in the extremes.

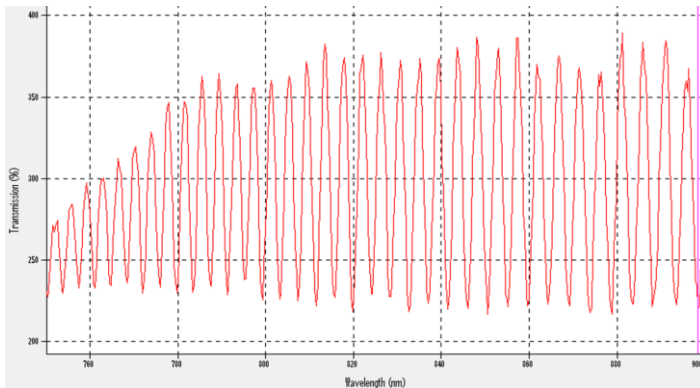


Figure 29. Interference pattern created by the reflected light.

6.2.4 Control of temperature

As it has been discussed, lyotropic LCs properties change broadly not only with the concentration, but also with the temperature. This is why the temperature has to be controlled. Furthermore, measurements of the nematic drops had to be performed at a constant temperature and at higher temperatures than room temperature.

For samples that were not under a magnetic field, the temperature was controlled with a homemade Peltier cell connected to an Aim-TTi EL302-USB Bench Power Supply. The Peltier cell had a sensor based on platinum whose electrical resistivity changed linearly with temperature. Hence, by measuring the resistance opposed by this sensor, the computer could know the exact temperature and could send signals to either heat or cool the cell. The software used to control the temperature was programmed with LabView.

When we worked with a magnetic field, samples were placed inside a thermostatic oven built with Thorlabs SM1 tube components and tape heater, and regulated with a Thorlabs TC200 controller.

6.2.5 Application of a magnetic field

To see the influence of a magnetic field to SY, samples with PVA-coated slides were placed between an array of magnets that produced a uniform magnetic field up to 4 kG parallel to the substrate. This array could rotate as it was connected to a rotor. The temperature was also controlled.

6.3 SY NEMATIC DROPS CHARACTERIZATION

LC cells were observed with a polarized light microscope Nikon Eclipse E400 POL with 10x and 20x objectives and a red light filter (RG-645-50.8 filter from Lambda), using a Pixelink PL-A741 camera for images in black and white and a Logitech C920 camera for the colored images.

For the study of SY in a magnetic field, it was used a customized inverted POM microscope with a LED light source from Thorlabs.

Images's processing was performed with the software ImageJ and curve fitting with IgorPro.

6.3.1 Twist angle measurements

Observations of the SY nematic drops were performed with LC cells with PVA-coated substrates under a POM microscope. In order to see the nematic drops, first we had to heat the LC cells until reaching the isotropic phase. Afterwards, the cells were let cooled down until seeing the nematic drops. Then the temperature had to be kept constant.

We could see that SY drops presented a twisted bipolar configuration, so that, we determined their twist angle.

It is possible to determine this angle by using optical methods. We used the method described by Jeonga et al. (ref. 14) that consisted on measuring the light intensity at the center of a drop at different analyzer/polarizer angles. Then, these values were fitted to a curve.

To see more in detail the method used, go to appendix 2.

6.3.2 Pitch measurements

Different samples of SY with different concentrations of brucine sulfate between PVA-coated slides were observed. It was seen that with brucine sulfate SY presented structures characteristic of cholesteric LCs. In this way, we determined one of the parameters used to characterize this kind of LC: the pitch. We used two different methods.

Method 1

For this method, a thin film of 0.9 m solution of SY with sulfate brucine at concentrations of 0.04%, 0.02% and 0.01% (wt.) was placed between a rubbed and a PVA-coated glass slides. The glass scratching produced a non-degenerate planar anchoring, hence the rubbing direction fixed the direction of the \mathbf{n} director at the surface, while at the other substrate the PVA-coated glass produced a degenerate planar anchoring i.e. it did not force a specific direction at the surface, except a parallel direction.

The LC cell was positioned in such a way that the rubbing direction was parallel to the analyzer. In this case, we worked with just the nematic phase (i.e. there were no nematic drops). Then, the polarizer was rotated while taking pictures at different angles of this optical element. The \mathbf{n} director's angle at the surface of the PVA-coated glass was the one that produced a minimum transmittance. Then, the pitch could be derived using the equation below:

$$p = \frac{360 \cdot d}{\alpha} \quad \text{Equation 3}$$

where d is the cell's thickness and α is the polarizer's angle.

This method is suitable just for LC presenting a pitch smaller than $d/2$. This is why we just used samples with small concentrations of sulfate brucine.

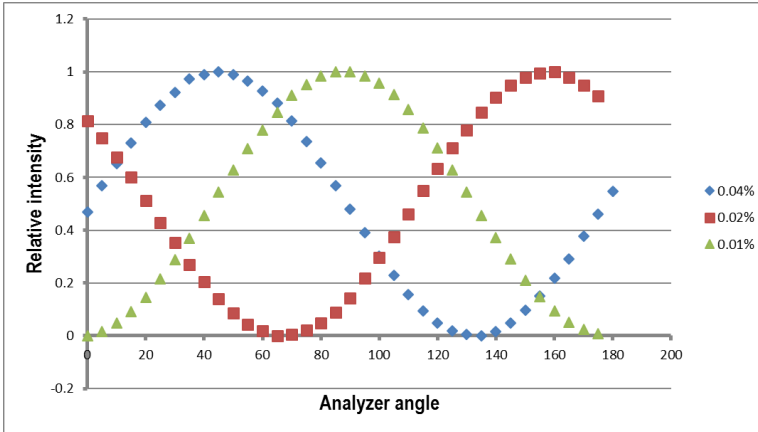


Figure 30. Light intensity arriving to the analyzer depending on the analyzer angle for different concentrations of brucine sulfate. The angle with a minimum intensity corresponds to the angle between the directors \mathbf{n} at opposite slides.

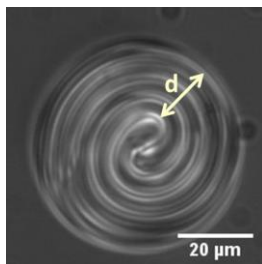
Method 2

For this method, different samples of 0.9 m solutions of SY with concentrations of 0.25%, 0.6%, 0.9%, 1.2% and 1.3% were sandwiched between two PVA-coated slides and were observed under a POM microscope. Here we did measure the pitch directly with the drops. At room temperature these samples did not present nematic drops, hence, in order to see the drops, we had to proceed as explained in section 9.3.1.

When seeing cholesteric drops with a POM microscope, it is possible to see that they present a texture which remembers to undulations. From one undulation to another, the \mathbf{n} director field twists a total angle of 180° . Hence, by measuring the distance between undulations it is possible to determine the pitch using the following equation:

$$P = \frac{2 \cdot d}{\text{number of undulations}} \quad \text{Equation 4}$$

where d is the distance between undulations.



$$P = \frac{2d}{\text{number of undulations}} = \frac{2d}{3}$$

Figure 31. Example of the determination of the pitch by method 2 using a POM image of a Frank-Price drop.

7. CONCLUSIONS

SY chemical structure makes possible the formation of a LCLC. We studied how this mesophase can be tuned by magnetic fields and chiral dopants. More specifically, we investigated the control in the coexistence region between the nematic and the isotropic phase of this LC.

In this coexistence region aforementioned, SY molecules performed a spherical configuration in order to minimize the surface tension. The way SY's molecules adapt themselves to this structure, depends on the three elastic constants and external fields, as a magnetic field.

In order to see how the drops configuration changed, we studied this configuration for pure SY. We observed that SY drops presented a twisted bipolar structure. This is because K_2 is small compared to the two other constants, favoring the twist distortion in front of splay and bend distortions. Furthermore, we also determined the twist angle of these droplets and its dependence with the concentration. Contrary to what we had expected, this angle seems not to vary depending on the concentration.

In the presence of a magnetic field, SY droplets changed their structure adopting a concentric configuration rather than a twisted bipolar configuration. This fact is due to the negative magnetic anisotropy of SY that makes the molecules to point perpendicular to the field, being the concentric configuration the one that best permits this alignment.

Finally, SY was doped with brucine sulfate, a chiral compound which induced a cholesteric mesophase. It was possible to see the typical oily streak texture and the Frank-Price drop configuration of chiral nematics. The pitch of this mesophase was determined and also its dependence with the chiral dopant's concentration, observing an increase of the chiral character with the concentration. Furthermore, we also saw that brucine sulfate leads the LC to twist in counterclockwise direction.

8. REFERENCES AND NOTES

- [1] OSWALD, P. and PIERANSKI, P. *Nematic and cholesteric Liquid Crystals*. Taylor and Francis, Boca Raton (2005)
- [2] Nobelprize.org *Liquid Crystals*. In Nobel Media AB 2014. Retrieved on April 2, 2016 from: http://www.nobelprize.org/educational/physics/liquid_crystals/history/
- [3] SHIYANOVSKII, S. V.; LAVRETOVICH, O. D.; SCHNEIDER, T.; ISHIKAWA, T.; SMALYUKH, I. I.; WOOLVERTON, C. J.; NIEHAUS, G. D. and DOANE, K. J. *Lyotropic Chromonic Liquid Crystals for Biological Sensing Applications*. *Mol. Cryst. Liq. Cryst.*, **434**, 259-270 (2005)
- [4] PARK, H. and LAVRETOVICH, O. D. *Liquid Crystals Beyond Displays: Chemistry, Physics and Applications*. John Wiley & Sons, INC. 449-483 (2012)
- [5] CHAMI, F. and WILSON, R. M. *Molecular Order in a Chromonic Liquid Crystal: A Molecular Simulation Study of the Anionic Azo Dye Sunset Yellow*. *J. Am. Chem. Soc.* **132**, 7794-7802 (2010)
- [6] SENYUK, B. *Liquid Crystals: a Simple View on a Complex Matter*. In Personal.kent.edu. Retrieved on March 4, 2016 from: <http://www.personal.kent.edu/~bisenyuk/liquidcrystals/index.html>
- [7] JÉROME, B. *Surface effects and anchoring in liquid crystals*. *Rep. Prog. Phys.* **54**, 391-451(1991)
- [8] *Anisotropy*. (n.d.) In Wikipedia. Retrieved on May 25, 2016 from: <https://en.wikipedia.org/wiki/Anisotropy>
- [9] LOPEZ-LEON, T. and FERNANDEZ-NIEVES, A. *Drops and shells of liquid crystal*. *Colloid Polym. Sci.* **289**, 345-359 (2011)
- [10] HASELOH, S.; VAN DER SCHOOT, P. and ZENTEL, R. *Control of mesogen configuration in colloids of liquid crystalline polymers*. *Soft Matter* **6**, 4112-4119 (2010)
- [11] CRAWFORD, G. P. and ZUMER, S. *Liquid Crystals In Complex Geometries: Formed by Polymer And Porous Networks*. Taylor & Francis (1996)
- [12] YANG, L.; KHAN, M. and PARK, S. *Liquid crystal droplets functionalized with charged surfactant and polyelectrolyte for non-specific protein detection*. *RSC Adv.* **5**, 97264-97271 (2015)
- [13] LEE, J.; KAMAL, T.; ROTH, S. V.; ZHANG, P. and PARK, S. *Structures and alignment of anisotropic liquid crystal particles in a liquid crystal cell*. *RSC Adv.* **4**, 40617-40625 (2014)
- [14] JEONG, J.; DAVIDSON, Z. S.; COLLINGS, P. J.; LUBENSKYA, T. C. and YODH, A. G. *Chiral symmetry breaking and surface faceting in chromonic liquid crystal droplets with giant elastic anisotropy*. *PNAS* **111**, 1742-1747 (2014)
- [15] AGUIRRE, L. E.; de OLIVEIRA, A.; SEC, D.; COPAR, S.; ALMEIDAA, P. L.; RAVNIKB, M. R.; GODINHOA, M. H. and ZUMER, S. *Sensing surface morphology of biofibers by decorating spider silk and cellulosic filaments with nematic microdroplets*. *PNAS* **113**, 1174-1179 (2016)

- [16] ORLOVA, T.; ABHOFF, S. J.; YAMAGUCHI, T.; KATSONIS, N. and BRASSELET, E. *Creation and manipulation of topological states in chiral nematic microspheres*. Nature Communications **6**, 7603 (2015)
- [17] YAO, X.; NAYANI, K.; PARK, J. O. and SRINIVASARAO, M. *Orientalional Order of a Lyotropic Chromonic Liquid Crystal Measured by Polarized Raman Spectroscopy*. J.Phys. Chem. B., Just Accepted Manuscript. (April 2016)
- [18] ROBINSON, P. C. and DAVIDSON, M. W. *Introduction to Polarized Light Microscopy*. In MicroscopyU from Nikon. Retrieved May 29, 2016 from: <http://www.microscopyu.com/articles/polarized/polarizedintro.html>
- [19] MURPHY, D. B.; SPRING, K. R.; FELLERS, T. J. and DAVIDSON, M. W. *Introduction to optical birefringence*; In MicroscopyU from Nikon. Retrieved on May 25, 2016 from: <http://www.microscopyu.com/articles/polarized/birefringenceintro.html>
- [20] *Retardation Plate Theory*. (n.d.) In Special Optics [PDF document] Retrieved on May 12, 2016 from: <http://www.somesite.com/>
- [21] YEH, P. and GU, C. *Optics of Liquid Crystal Displays*. Wiley, Hoboken, NJ (2009)
- [22] JEONG, J.; HAN, G.; JOHNSON, A.T. C.; COLLINGS, P. J.; LUBENSKY, T., C. and YODH, A. G. *Homeotropic Alignment of Lyotropic Chromonic Liquid Crystals Using Noncovalent Interactions*. Langmuir **30**, 2914–2920 (2014)
- [23] GOTTARELLI, G.; HIBERT, M.; SAMORI, B.; SOLLADI, G.; SPADA, G. P. and ZIMMERMANNLE, R. *Induction of the Cholesteric Mesophase in Nematic Liquid Crystals: Mechanism and Application to the Determination of Bridged Biaryl Configurations*. J. Am. Chem. Soc. **105**, 7318-7321(1983)
- [24] CELEBRE, G.; DE LUCA, G.; MAIORINO, M.; IEMMA, F.; FERRARINI, A.; PIERACCINI, S. and SPADA, G. P. *Solute-Solvent Interactions and Chiral Induction in Liquid Crystals*. J. Am. Chem. Soc. **127**, 11736–11744 (2005)
- [25] KITZEROW, H. and BAHR, C. *Chirality in Liquid Crystals*. Springer Science & Business Media, 1st Edition (2001)
- [26] CUI, Y.; *Polymer's anchoring behavior in liquid crystal cells*. From Kent University (2014) [PDF document] Retrieved on 29th May 2016 from: https://etd.ohiolink.edu/etd.send_file?accession=kent1406515363&disposition=inline
- [27] HOROWITZ, V. R. ; JANOWITZ, L. A.; MODIC, A. L.; HEINEY, P. A. and COLLINGS, P. J. *Aggregation behavior and chromonic liquid crystal properties of an anionic monoazo dye*. Phys. Rev. E **72**, 041710 (2005)

9. ACRONYMS

LC: Liquid crystals

SY: Sunset yellow

LCLC: Lyotropic chromonic liquid crystals

POM: Polarized optical microscope

TN-LCD: Twisted Nematic liquid display

APPENDICES

APPENDIX 1: DEFECTS IN NEMATIC DROPS

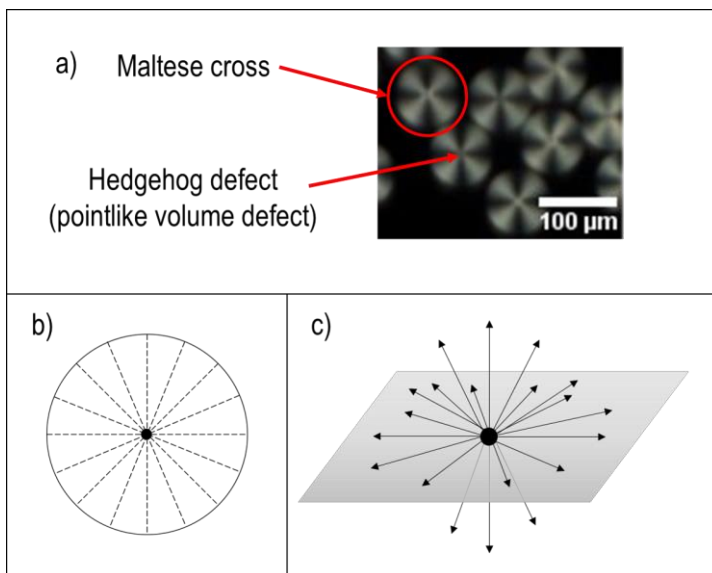


Figure 32. POM image of radial drops (a), representation of the director field in the drop equator seen perpendicularly to the principal axis, the black dot indicates the hedgehog defect (b); representation of the director \mathbf{n} field around the hedgehog defect (c). Image a is adapted from Yang et. al. (ref. 12) with permission of The Royal Society of Chemistry

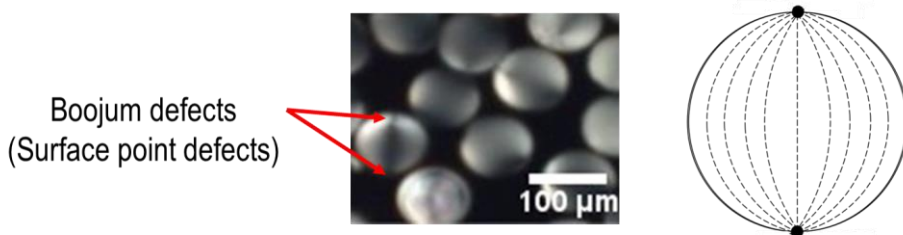


Figure 33. Boojum defects of bipolar drops seen in a POM microscope (left) and a representation of the lines of the director \mathbf{n} field seen parallel to the principal axis, the black dots indicate the two boojums (right). The POM image is adapted from Yang et. al. (ref. 12) with permission of The Royal Society of Chemistry

Equatorial disclination
ring on the surface

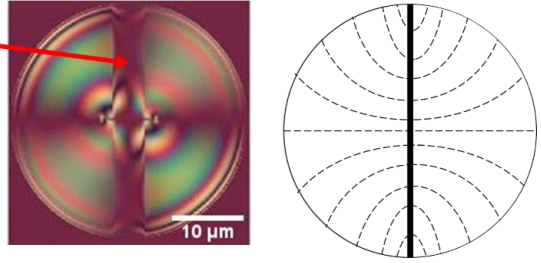


Figure 34. The ring defect of an axial drop seen in a POM microscope (left) and a representation of the lines of the director n field seen parallel to the principal axis, the black dots indicate the two boojums (right). The POM image is adapted from Aguirre et. al. (ref. 15)

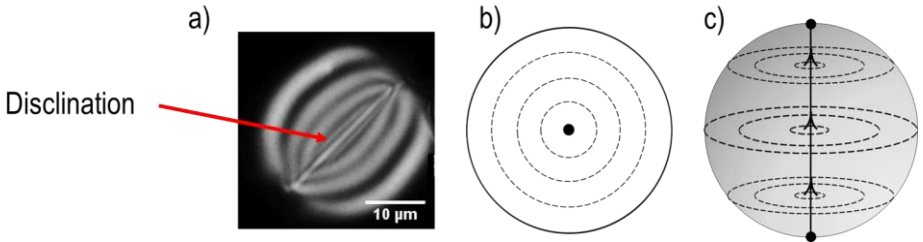


Figure 35. Disclination line defect of a concentric drop in a POM microscope (a), representation of the director n field at the equator of the drop perpendicular to the principal axis, the black dot indicates the disclination at the principal axis (b) and representation of the disclination (c). The POM image is adapted from Jeong et. al. (ref. 14)

Hedgehog
(pointlike volume defect)

Dirac string
(disclination)

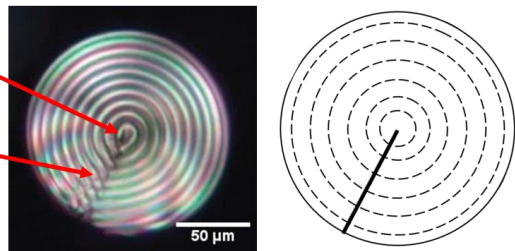


Figure 36. The two typical defects (hedgehog defect and Dirac string) of Frank-Price drops seen in a POM microscope (left) and a representation of the lines of the director n field at the equator of the drop, the black line indicates the Dirac string (right). The POM image is adapted from Orlova et. al. (ref. 16)

APPENDIX 2: TWIST ANGLE CHARACTERIZATION METHOD

As was previously mentioned, we used the method described by Jeong et al. (ref. 14) in order to determine the twist angle of the twisted bipolar drops.

Here it can be found a brief explanation of the method used. However, before explaining it, we will make a brief description of the Jones matrix calculus as it will be needed in order to give a good explanation.

Jones calculus²¹

In 1941 Robert Clark Jones invented a calculus for describing the transmission of birefringent materials. Polarized light is described by a two-component vertical vector (the Jones vector) and the optical elements, as a plate retarder, by a 2x2 matrix (the Jones matrix). With this method, it's possible to predict how polarized light would be newly polarized when crossing an optical element, which can be constructed with birefringent media. The mathematical expression is the one below:

$$\begin{pmatrix} V_x^{out} \\ V_y^{out} \end{pmatrix} = \begin{pmatrix} M_{11} & M_{12} \\ M_{21} & M_{22} \end{pmatrix} \begin{pmatrix} V_x^{in} \\ V_y^{in} \end{pmatrix} \quad \text{Equation 5}$$

V_x^{out} and V_y^{out} are the light components that exit the optical element and V_x^{in} and V_y^{in} the ones that enter. If the light goes through more than one optical element, then the Jones matrix can be written as the product of all individual Jones matrices.

Transmission through a twisted nematic LC display

Jeong et al. (ref 14.) proposed a method in which the twisted bipolar nematic drops were seen as TN-LCD (Twisted Nematic- Liquid Crystal Displays). TN-LCDs are optical elements that are composed by twisted nematic mesophases and these LCs have the singularity that the n director turns along a perpendicular axis.

The transmittance in TN-LCD was described by the method proposed by Yeh et. al. (ref. 14). So that, we will first explain the method of Yeh et. al.

In this model, they supposed that TN-LCD were created by stacking several retardation plates with equally phase retardation. Each plate had an orientation which corresponded to the \mathbf{n} director of the nematic forming the plate and, this orientation changed a given angle (ρ) from one plate to the next one. Hence, the total twist angle (the angle that the \mathbf{n} director turned from one substrate to the other) was given by $\Phi=N \cdot \rho$.

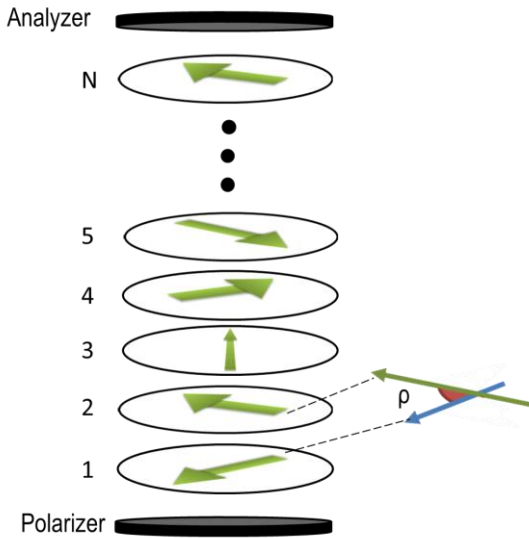


Figure 37. Representation of the N plates and the ρ and Φ angles. The green arrows represent the director \mathbf{n} at every plate (Note: \mathbf{n} and $-\mathbf{n}$ directors in nematics are equivalent). All the plates have the same phase retardation.

Then, they defined a Jones matrix for each plate (W_m), so that, the overall Jones Matrix (M) was defined as the product of these Jones matrices:

$$M = W_N W_{N-1} \cdots W_3 W_2 W_1 = \prod_{m=1}^N W_m \quad \text{Equation 6}$$

With $N \rightarrow \infty$ and:

$$T = |V'^* \cdot MV|^2 \quad \text{Equation 7}$$

where V' and V are the input and output Jones vectors, respectively (Note: V'^* is the conjugated vector of V') and doing some algebraic calculus, they arrived to the following expression for the light transmission:

$$T = \cos^2(\phi - \Phi_{exit} + \Phi_{ent}) + \sin^2\phi \sin 2(\phi - \Phi_{exit}) \sin 2\Phi_{ent} \quad \text{Equation 8}$$

where Φ_{ent} is the angle between the analyzer director and the \mathbf{n} director of the first plate and Φ_{exit} is the angle between the same \mathbf{n} director and the polarizer director.

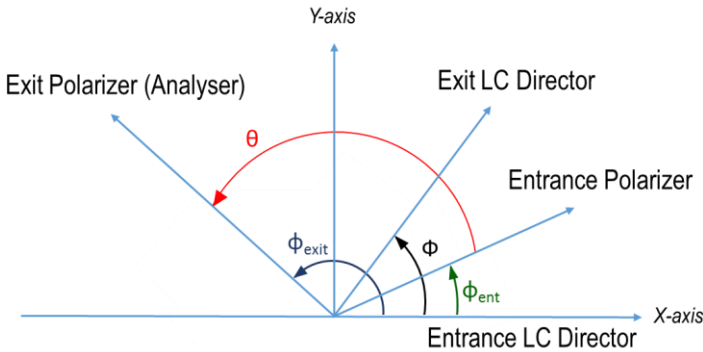


Figure 38. Schematic drawing showing the orientation of the polarizer axes, LC directors of a general TN-LCD in the xy plane. The x axis (the reference axis) is chosen as the entrance LC director orientation. All angles are measured from the x axis.

However, this model was for planar surfaces and in this study the surfaces were curved. In this way, it had to be adapted.

Transmission through twisted bipolar drops

We supposed that the center of the drops was planar i.e. curvature was neglected. So that, in order to minimize the error made with this approximation, the light intensity was measured just at a small region at the center of the drop. We also supposed that there was symmetry around the principal axis of the drops, meaning that at the center the director \mathbf{n} field laid along this axis and from this axis towards the surface, the director \mathbf{n} twisted the same angle as towards the opposite surface, but in the other direction.

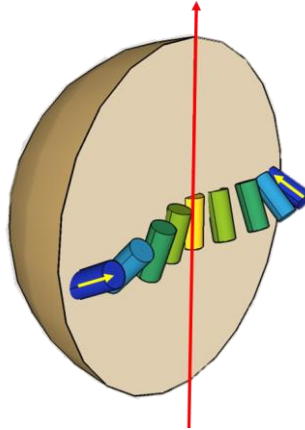


Figure 39. Schematic representation of the mesogens along the principal axis.

Then, our axes were defined as it can be seen in the following figure:

Angle at LC entrance LC: $-\alpha_0$

Angle of polariser: α_{pol}

Angle of analyser: α_{an}

$$\phi_{ent} = \alpha_{pol} - (-\alpha_0) = \alpha_{pol} + \alpha_0$$

$$\phi_{exit} = \alpha_{an} - (-\alpha_0) = \alpha_{an} + \alpha_0$$

$$\theta = \alpha_{an} - \alpha_{pol}$$

$$\Phi = \alpha_0 - (-\alpha_0) = 2\alpha_0$$

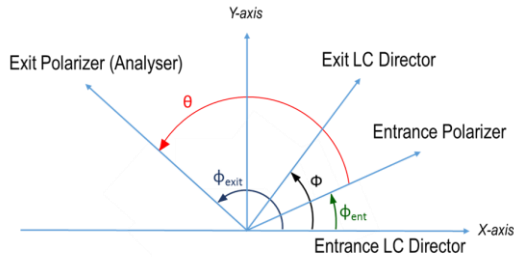


Figure 40. Representation of the orientation of the different axes. Emphasize that as we supposed that the drop was symmetric around the principal axis, we could write $\phi = 2\alpha_0$ were α_0 would be the angle that the director n twisted from the center towards the surface. This angle is the so-called twist angle.

Finally, we added another angle to the angle system that related the orientation of the drop's principal axis with the orientation of the polarizer. This angle was β . The final function that we used to make the curve fitting was:

$$I(\theta) = A + B[\cos^2(2\alpha_0 - \theta) + \sin^2(\chi) \cdot \sin 2(\alpha_0 + \alpha_{pol} + \beta) \cdot \sin 2(\alpha_{pol} + \alpha_0 + \beta)] \quad \text{Equation 9}$$

where χ is given as:

$$\chi = \sqrt{(2\alpha_o)^2 + \left(\frac{\pi \cdot \Delta n \cdot d}{\lambda}\right)^2} \quad \text{Equation 10}$$

where Δn is the birefringence, d the drop diameter and λ the wavelength.

Δn values were taken from Horowitz et. al. (ref. 27) and λ was taken as $0.76 \mu\text{m}$ since we used just red light for these measurements.

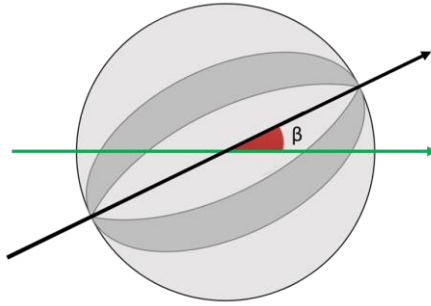


Figure 41. Representation of the β angle. The green arrow indicates the polarization director of the polarizer and the black arrow the principal axis of a drop.

To sum up, in order to find the twist angle (α_0), we measured the intensity of the light at the center of different drops at different angles between the analyzer and the polarizer. It has to be remarked that the only drops which could be analyzed were the ones that were disposed in such a way that the principal axis laid parallel to the substrates. Then, these values were fitted to Equation 10.

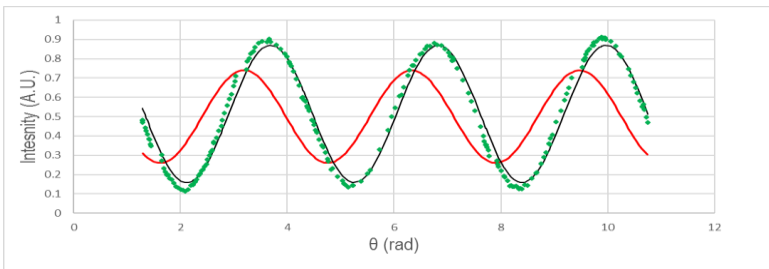


Figure 42. Curve fitting (in black) of the experimental results (dots in green) using equation. The plot in red represents a calculation of the intensity supposing $\alpha_0=0$

